Chapter 5

Simulation of two dimensional dam break problem with variable bottom geometry

5.1 Introduction

Shallow water equations represent a nonlinear system of conservation laws having some features of more complicated systems such as gas dynamic equations. These equations are hyperbolic in nature and act as a basis for many mathematical models for simulation of fluid flow processes. These equations arise in wide range of physical phenomena such as free surface flows, dam break flows, tidal bores and river flood etc., Stoker (1957).

The problems occurring in real life situations have no analytical solution, owing to the nonlinearity of the model and complexity of the geometries involved. In recent years, considerable efforts have been made to develop the numerical methods for solving the equations approximately (Toro (1992) and (2001), Zhou et al. (2002), Murillo et al., (2010) and Toro (2001)). Godunov method (1959) forms the basic building block for most of the well-known numerical schemes for conservative systems. Godunov type methods require the solution of Riemann problem at the cell interfaces. The use of approximate analytical solutions of Riemann problem requires a large number of computations at each cell interface. To avoid this situation, approximate Riemann solvers are used. One of the most well-known approximate Riemann solvers is the Roe solver (1981) and the HLL solver presented by Herten et al. (1983). In the Roe solver

---

The contents of this chapter are communicated for the publication

the Jacobian matrix of the hyperbolic system is replaced with approximate Jacobian matrix. The solution is obtained by decomposing the flux vector in to positive and negative components. The HLL solver is derived by considering two waves at the point of discontinuity with an intermediate state in between. The numerical flux results directly from governing equations. HLL method takes care of only two propagating waves, a valid assumption for one dimensional flow with two variables. In case of two or three dimensions the number of variables and equations increases, leading to two intermediate states separated by a contact discontinuity. Toro *et al.* (1994) extended the HLL method to incorporate the contact wave and the method is known as HLLC method. Another scheme for conservative systems is the Random Choice Method introduced by Glimm (1965) and developed and applied successfully by Chorin (1976). It has also been successfully applied to shallow water equations with flat bottom, Miniati (2007). The Random Choice Method and the Godunov method are theoretically same except the sampling procedure. The Godunov method uses the integral average of solution of Riemann problem in each cell whereas RCM picks a single state, contained in the local solutions, at random. The random sampling is performed by incorporating a sequence of random numbers, see Colella (1982). The distinguished feature of RCM is its ability to resolve shock waves and contact discontinuities, see Colella (1982). Recently Random Choice Method has been used for simulation of dam break problem for shallow water equations by Himanshu et al. (2015). Miniati (2007) numerically solved the equations for cosmic – ray hydrodynamics using Glimm's and Godunov methods. Further works on shallow water equations can be found in Concus et al. (1979) and Hong et al. (2006). The FORCE (First Order Centered Deterministic) scheme is obtained by replacing the stochastic steps of the Random choice method with deterministic versions, using the integral averages of the Riemann problem solutions.

The FORCE method is although first order, it has optimal stability conditions for explicit methods and has the smallest numerical viscosity. It is shown by Chen et al., (2004) that the FORCE scheme is consistent with the Lax entropy conditions, and for one dimensional shallow water equations the solution via FORCE scheme converge to the original solutions.

In recent decades, many authors have presented approximate and exact solutions for shallow water equations; see Thacker, (1981), Bernetti et al. (2008) and Alcrudo et al. (2001) that may be helpful in checking validity of numerical methods. In real life problems the system of shallow water equations include source terms due to bed variation, bottom friction etc. Many efforts have been made to deal with source terms. Bermudez and Vazquez-Cendon (1994) used the upwind treatment of source term to produce better result in comparison to the pointwise method for rectangular channel with bed variation. Garcia Navarro and Vazquez-Cendon (2000), Hubbard and Garcia Navarro (2000) applied the upwind treatment to high resolution schemes. Lee and Wright (2010) integrated the source terms by a straight forward modification of the governing equations. To ensure well balanced property Zhou et. al. (2001) used the water surface gradient as the basis for data reconstruction. Liang and Borthwick (2009) formulated a second order scheme by writing the set of equations in a deviatory form and used the two step unsplit MUSCL-Hancock method in combination with the HLLC solver. Yulong and Chi-Wang (2005) designed a well-balanced finite difference high order WENO Lax Friedrich scheme, without reducing the higher order accuracy. Murillo and Garcia Navarro (2012) developed the HLLS and HLLCS Riemann solvers by including an extra wave in the original HLL and HLLS solvers.

In the present chapter, we have successfully applied the FORCE method for the numerical simulation of two dimensional shallow water equations with variable bottom

geometry. The obtained numerical results are compared with existing analytical and numerical solutions. An effort has been made to show that in case of operator splitting for multi-dimensional flow, there is no uniform approximation to the bed slope. Further, the FORCE method is applied to multidimensional flow problems and it was observed that in case of multidimensional flow the treatment of source term depends upon the geometry of the problem.

5.2 Governing equations

The two dimensional shallow water equations with discontinuous bottom topography in cartesian coordinate system are given as, (Murillo et al., (2010))

$$\frac{\partial U}{\partial t}+\frac{\partial F}{\partial x}+\frac{\partial G}{\partial y}=S(U), \tag{5.1}$$

in which,

$$U=\begin{bmatrix} h \\ hu \\ hv \\ z \end{bmatrix},\ F=\begin{bmatrix} hu \\ hu^2+gh^2/2 \\ huv \\ 0 \end{bmatrix},\ G=\begin{bmatrix} hv \\ huv \\ hv^2+gh^2/2 \\ 0 \end{bmatrix},\ S=\begin{bmatrix} 0 \\ -ghz_x \\ -ghz_y \\ 0 \end{bmatrix}, \tag{5.2}$$

where h is the height of water level, u and v are the velocity components in x and y direction respectively, z is the bottom elevation and g is the acceleration due to gravity. U is the vector of conserved variables, F is the flux in $x-$direction and G is the flux in $y-$ direction and S is the source term vector.

5.3 One dimensional flow and Riemann problem

Many hydraulic problems can be explained via one dimensional model. The equations for one dimensional model can be obtained by neglecting y components from equation (5.1). The one dimensional equations to model unsteady flow in a channel of variable depth can be written as

$$\begin{bmatrix} h \\ hu \\ z \end{bmatrix}_t + \begin{bmatrix} hu \\ hu^2 + gh^2/2 \\ 0 \end{bmatrix}_x = \begin{bmatrix} 0 \\ -ghz_x \\ 0 \end{bmatrix}. \tag{5.3}$$

The initial conditions for the Riemann problem for (5.3) are

$$U(x,0) = \begin{cases} U_L, \text{if } x < 0 \\ U_R, \text{if } x > 0 \end{cases}, \tag{5.4}$$

where $-\infty < x < \infty,\ t > 0$. We can take x to vary in a finite interval $[a, b]$ around the point $x = 0$. Initial data for the Riemann problem (5.3)-(5.4) consists of two constant states, which are (h_L, u_L, z_L) to the left of $x = 0$ and (h_R, u_R, z_R) to the right of $x = 0$, separated by a discontinuity at $x = 0$. Setting $V^t = (h, u, z)$, equation (5.3) can be written as

$V_t + A(V)V_x = 0$,

where the jacobian matrix $A(V)$ is given as

$$A = \begin{bmatrix} u & h & 0 \\ g & u & g \\ 0 & 0 & 0 \end{bmatrix}. \tag{5.5}$$

The Jacobian matrix has three real eigenvalues $\lambda_0 = 0,\ \lambda_1 = u - c,\ \lambda_2 = u + c,$ with eigenvectors $e_0 = \left(\frac{c^2 - u^2}{c^2}, 1, -\frac{u}{h}\right)^t, e_1 = \left(0, 1, -\frac{c}{h}\right)^t, e_2 = \left(0, 1, \frac{c}{h}\right)^t,$ where $c = \sqrt{gh}$ is the wave celerity. The given nonlinear system of equations is strictly hyperbolic. The situation can be represented in the $x - t$ plane as shown in the figure 5.1.

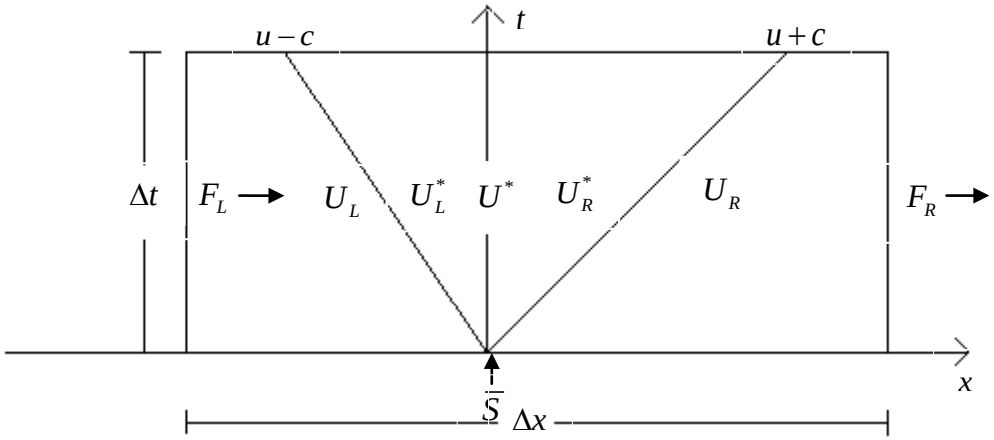

Figure 5.1 Wave pattern for the solution of the Riemann problem for one dimensional shallow water equations.

Physically, it represents one dimensional dam break problem with variable bottom. When the dam is broken, it suddenly produces a nearly centered wave system consisting of a rarefaction wave, a stationary contact discontinuity and/or a shock (bore) wave. The three waves given by $\lambda_0 = u - c,\ \lambda_1 = 0,\ \lambda_2 = u + c,$ separate four constant states namely U_L to the left of the left wave, U_R to the right of the right wave and two new constant states U_L^* and U_R^*, to the left and right of the stationary wave, valid in the region between the left and right waves.

5.4 Numerical solution

The domain under consideration can be taken to be $[0, L] \times [0, M]$. The domain $[0, L], [0, M]$ has been discretized in x and y directions respectively into N , K grid cells $I_i = \left[x_{i-\frac{1}{2}}, x_{i+\frac{1}{2}} \right]$, $J_i = \left[y_{i-\frac{1}{2}}, y_{i+\frac{1}{2}} \right]$ of size L / N for x-direction and M / K in y-direction respectively. Here, Δx is the step size in x-direction, Δy is the step size in y-direction.

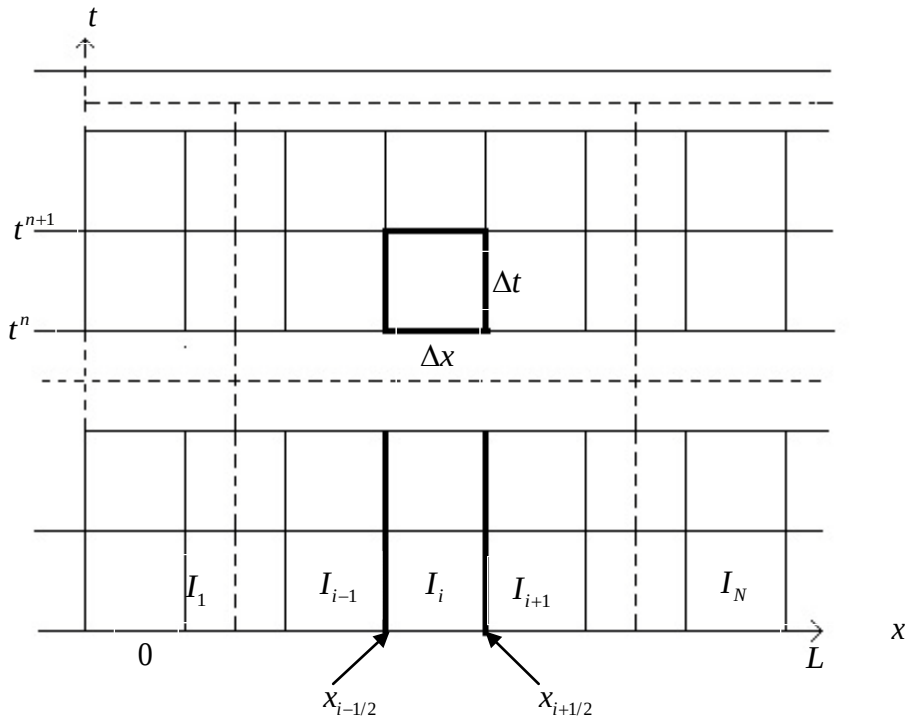

Figure 5.2 The grid discretization in the x-direction.

5.4.1 Method of solution

We solve equation (5.3) by using an operator splitting procedure following (Toro, 2009). The hyperbolic conservation law with source term

$$\begin{aligned} &U_t + F(U)_x = S(U), \\ &U(x,t^n) = U^n, \end{aligned} \tag{5.6}$$

can be solved by breaking it into the advection problem

$$\begin{aligned} &U_t + F(U)_x = 0, \\ &U(x,t^n) = U^n, \end{aligned} \tag{5.7}$$

and transient problem

$$\frac{dU}{dt} = S(U),\ U(0) = \bar{U}^{n+1}, \tag{5.8}$$

where $\bar{U}^{n+1}$ is the solution of the homogeneous problem (5.7).

The homogeneous problem (5.7) can be solved numerically by utilizing an explicit conservative method of Godunov type (for non-linear hyperbolic systems) to get

$$\bar{\mathrm{U}}_i^{n+1} = \mathrm{U}_i^n + \frac{\Delta t}{\Delta x}(\mathrm{F}^n_{i-\frac{1}{2}} - \mathrm{F}^n_{i+\frac{1}{2}}). \tag{5.9}$$

The equation (5.8) can be solved by using Euler or Runge-Kutta methods, See Toro (2009).

Thus, the final solution of (5.6) is given by

$$\begin{aligned} \bar{U}_i^{n+1} &= U_i^n + \frac{\Delta t}{\Delta x}\left(F^n_{i-\frac{1}{2}} - F^n_{i+\frac{1}{2}} \right), \\ U_i^{n+1} &= \bar{U}_i^{n+1} + \Delta t S(\bar{U}_i^{n+1}) \end{aligned} \tag{5.10}$$

where, U is the vector of conserved variables, $\bar{U}$ is the solution of the homogeneous equation, S is the source term and F is the numerical flux at the cell interface $i+1/2$ and $i-1/2$ given by

$$F^n_{i+\frac{1}{2}} = F\left(U^n_{i+\frac{1}{2}}(0) \right),\ F^n_{i-\frac{1}{2}} = F\left(U^n_{i-\frac{1}{2}}(0) \right), \tag{5.11}$$

where, $U^n_{i+\frac{1}{2}}(0)$ and $U^n_{i-\frac{1}{2}}(0)$ represents the solution of local Riemann problem $RP\left(\mathrm{U}_i^n, \mathrm{U}_{i+1}^n\right)$ and $RP\left(\mathrm{U}_{i-1}^n, \mathrm{U}_i^n\right)$ respectively along the line $x/t = 0$.

5.4.2 Random Choice Method

The Random Choice Method was proposed by Glimm (1965), for the solution of a class of nonlinear hyperbolic system of conservation laws.There are two prerequisites for the application of RCM (i) solution of local Riemann problem at each cell interface and (ii) a sampling procedure to randomly select the states to be assigned for the next level computation. The RCM assumes a piecewise constant distribution of data in each cell I_i.

For a given initial state $U(x,t^n)$, at time $t = t^n$, it is required to find the solution at time $t = t^{n+1}$. The method for non staggered grid is divided into two steps:

(i) Solve the local Riemann problems $RP\left(\mathrm{U}_i^n, \mathrm{U}_{i+1}^n\right), RP\left(\mathrm{U}_{i-1}^n, \mathrm{U}_i^n\right)$ arising due to the constant states $\mathrm{U}_{i-1}^n, \mathrm{U}_i^n, \mathrm{U}_{i+1}^n$ to find the solutions as $\hat{\mathrm{U}}_{i+\frac{1}{2}}^{n+\frac{1}{2}}(x,t)$ and $\hat{\mathrm{U}}_{i-\frac{1}{2}}^{n+\frac{1}{2}}(x,t)$ respectively.

(ii) Random sample these solutions at time $t = \Delta t^{n+1}$ for the solution in the cell I_i. The selected state depends upon the choice of a quasi-random number θ^n which lies in the interval $[0,1]$.

The solution is thus obtained as

$$\mathrm{U}_i^{n+1} = \begin{cases} \mathrm{U}_{i-\frac{1}{2}}(\theta^n \Delta x / \Delta t), & \text{if } 0 \le \theta^n \le \frac{1}{2} \\ \mathrm{U}_{i+\frac{1}{2}}((\theta^n - 1)\Delta x / \Delta t), & \text{if } \frac{1}{2} < \theta^n \le 1 \end{cases}. \tag{5.12}$$

Staggered cell division

The staggered grid version of RCM is the same as the non staggered version except that the random sampling procedure is applied in both the steps. More specifically, the solution is obtained in two steps as:

(i) Solve the local *Riemann Problems* $RP\left(\mathrm{U}_i^n, \mathrm{U}_{i+1}^n\right), RP\left(\mathrm{U}_{i-1}^n, \mathrm{U}_i^n\right)$ arising due to the constant states $\mathrm{U}_{i-1}^n, \mathrm{U}_i^n, \mathrm{U}_{i+1}^n$ the solution of which are obtained as $\hat{\mathrm{U}}_{i+\frac{1}{2}}^{n+\frac{1}{2}}(x,t)$ and $\hat{\mathrm{U}}_{i-\frac{1}{2}}^{n+\frac{1}{2}}(x,t)$ respectively.

Random sample these solutions at time $t = \Delta t^{n+\frac{1}{2}}$, to obtain the solutions as

$$\mathrm{U}_{i-\frac{1}{2}}^{n+\frac{1}{2}} = \hat{\mathrm{U}}_{i-\frac{1}{2}}^{n+\frac{1}{2}}(\theta^n \Delta x, \Delta t^{n+\frac{1}{2}}) \ , \ \mathrm{U}_{i+\frac{1}{2}}^{n+\frac{1}{2}} = \hat{\mathrm{U}}_{i+\frac{1}{2}}^{n+\frac{1}{2}}(\theta^n \Delta x, \Delta t^{n+\frac{1}{2}}). \tag{5.13}$$

(ii) Solve the Riemann Problem $RP\left(\mathrm{U}_{i-\frac{1}{2}}^{n+\frac{1}{2}}, \mathrm{U}_{i+\frac{1}{2}}^{n+\frac{1}{2}}\right)$ to get the solution $\hat{\mathrm{U}}_i^{n+1}(x,t)$ and random sample it at time $t = \Delta t^{n+1}$ to obtain the final solution as

$$\mathrm{U}_i^{n+1} = \hat{\mathrm{U}}_i^{n+1}(\theta^n \Delta x, \Delta t^{n+1}). \tag{5.14}$$

5.4.3 The FORCE Method

The FORCE (First Order Centered) scheme is the deterministic version of the original Random Choice Method on a staggered grid. It is obtained by replacing the stochastic steps of Random Choice Method with deterministic steps through integral averages of the Riemann problem solutions, see Toro (2009).

Let $\hat{\mathrm{U}}_{i+\frac{1}{2}}(x,t)$ and $\hat{\mathrm{U}}_{i-\frac{1}{2}}(x,t)$ be solutions of the local Riemann problem $RP\left(\mathrm{U}_i^n, \mathrm{U}_{i+1}^n\right)$ and $RP\left(\mathrm{U}_{i-1}^n, \mathrm{U}_i^n\right)$ respectively. Then, setting $\Delta t^{n+\frac{1}{2}} = \frac{1}{2}\Delta t$, we obtain the integral averages as

$$\mathrm{U}_{i-\frac{1}{2}}^{n+\frac{1}{2}} = \frac{1}{\Delta x}\int_{-\Delta x/2}^{\Delta x/2} \hat{\mathrm{U}}_{i-\frac{1}{2}}^{n+\frac{1}{2}}\left(x, \frac{\Delta t}{2}\right) dx, \tag{5.15}$$

and

$$\mathrm{U}_{i+\frac{1}{2}}^{n+\frac{1}{2}} = \frac{1}{\Delta x}\int_{-\Delta x/2}^{\Delta x/2} \hat{\mathrm{U}}_{i+\frac{1}{2}}^{n+\frac{1}{2}}\left(x, \frac{\Delta t}{2}\right) dx. \tag{5.16}$$

The integral form of conservation laws is applied to (5.15) and (5.16), to get

$$\mathrm{U}_{i-\frac{1}{2}}^{n+\frac{1}{2}} = \frac{1}{2}(\mathrm{U}_{i-1}^n + \mathrm{U}_i^n) + \frac{\Delta t}{2\Delta x}(\mathrm{F}_{i-1}^n - \mathrm{F}_i^n), \tag{5.17}$$

$$\mathrm{U}_{i+\frac{1}{2}}^{n+\frac{1}{2}} = \frac{1}{2}(\mathrm{U}_i^n + \mathrm{U}_{i+1}^n) + \frac{\Delta t}{2\Delta x}(\mathrm{F}_i^n - \mathrm{F}_{i+1}^n). \tag{5.18}$$

Next, let $\hat{\mathrm{U}}_i(x,t)$ be the solution of local Riemann problem $RP\left(\mathrm{U}_{i-\frac{1}{2}}^{n+\frac{1}{2}}, \mathrm{U}_{i+\frac{1}{2}}^{n+\frac{1}{2}}\right)$, then the

solution U_i^{n+1} is obtained by taking the integral average of $\hat{U}_i(x,t)$ at local time $t = \Delta t / 2$.

$$U_i^{n+1} = \frac{1}{\Delta x}\int_{-\Delta x/2}^{\Delta x/2} \hat{U}_i^n(x, \Delta t)dx. \tag{5.19}$$

Using integral form of conservation laws, (5.19) becomes

$$U_i^{n+1} = \frac{1}{2}(U_{i-\frac{1}{2}}^{n+\frac{1}{2}} + U_{i+\frac{1}{2}}^{n+\frac{1}{2}}) + \frac{\Delta t}{2\Delta x}(F_{i-\frac{1}{2}}^{n+\frac{1}{2}} - F_{i+\frac{1}{2}}^{n+\frac{1}{2}}) \quad , \tag{5.20}$$

where,

$$F_{i+\frac{1}{2}}^{n+\frac{1}{2}} = F(U_{i+\frac{1}{2}}^{n+\frac{1}{2}}) \equiv F_{i+\frac{1}{2}}^{RI} \ . \tag{5.21}$$

$F_{i+\frac{1}{2}}^{RI}$ is the Richtmyer Flux, see Toro (2009) calculated as

$$F_{i+\frac{1}{2}}^{RI} = F(U_{i+\frac{1}{2}}),$$

where, $U_{i+\frac{1}{2}}$ and $U_{i-\frac{1}{2}}$ are given by equation (5.18) and (5.17) respectively.

The equation (5.20) of FORCE Scheme can be written in conservative form

$$U_i^{n+1} = U_i^n + \frac{\Delta t}{\Delta x}(F_{i-\frac{1}{2}}^n - F_{i+\frac{1}{2}}^n) \quad , \tag{5.22}$$

with intercell numerical flux:

$$F_{i+\frac{1}{2}}^{force} = \frac{1}{2}\left[F_{i+\frac{1}{2}}^{n+\frac{1}{2}} + \frac{1}{2}\left(F_i^n + F_{i+1}^n\right)\right] + \frac{\Delta x}{4\Delta t}\left(U_i^n - U_{i+1}^n\right) \text{ and}$$

$$F_{i-\frac{1}{2}}^{force} = \frac{1}{2}\left[F_{i-\frac{1}{2}}^{n+\frac{1}{2}} + \frac{1}{2}\left(F_{i-1}^n + F_i^n\right)\right] + \frac{\Delta x}{4\Delta t}\left(U_{i-1}^n - U_i^n\right). \tag{5.23}$$

The above Flux is the arithmetic mean of the Richtmyer and Lax-Friedrichs Method

$$\mathrm{F}^{\text{force}} = \frac{(\mathrm{F}^{\mathrm{RI}} + \mathrm{F}^{\mathrm{LF}})}{2}. \tag{5.24}$$

5.4.4 Source term discretization

The variable bottom slope $\partial z/\partial x$ can be approximated by the central difference as suggested in Toro (1992)

$$\partial z/\partial x \approx (z_{i+1/2} - z_{i-1/2})/\Delta x, \tag{5.25}$$

or by forward difference type as

$$\partial z/\partial x \approx (z_{i+3/2} - z_{i-1/2})/(2\Delta x). \tag{5.26}$$

The formula (5.25) suggested in Toro (1992) gives good approximation to the bed slope for one dimensional flow but in case of two dimensional flow this approximation results in erroneous result. In this case, the application of the formula (5.26) gives good result.

5.4.5 Time Step

In the numerical solution of a conservation form of equations the time step Δt depends on intercell flux of the particular method, the wave speed(s) and the grid dimensions. It is defined as:

$$\Delta t = C_{cfl} \times \min_{i,j}\left(\frac{\Delta x_{i,j}}{S^{n,x}_{i,\mathrm{j},\mathrm{k}}}, \frac{\Delta y_{i,j}}{S^{n,y}_{i,j,k}}\right), \tag{5.27}$$

where, C_{cfl} is the CFL (Courant Friedrichs-Lewy) stability criteria which lies in the interval [0,1] according to the method chosen, in case of Force method C_{cfl} satisfies the condition $0 \le C_{cfl} \le 1$. $S^{n,\mathrm{d}}_{i,\mathrm{j}}$ represents the speed of the fastest wave at time step n travelling in d direction where $d = x \text{ or } y$. Here one requires the wave speed estimates only to determine the time step size. For this we have taken the estimate given in Toro (2009)

$$S_{i,j}^{n,d} = \max(u_{ij}^{n,d} - \sqrt{gh_{ij}^{n,d}}, u_{ij}^{n,d} + \sqrt{gh_{ij}^{n,d}}). \tag{5.28}$$

where, $u_{i,j}^{n,d}$ is the velocity component in d direction at time n and $h_{i,j}^{n,d}$ is the height at time n in the cell $I_{i,j}$.

5.5 Two Dimensional Case

Following Toro (2009), we solve the equation by using operator splitting procedure. Here, we first solve the x-split equations according to

$$\begin{bmatrix} h \\ hu \\ hv \end{bmatrix}_t + \begin{bmatrix} hu \\ hu^2 + gh^2/2 \\ huv \end{bmatrix}_x = \begin{bmatrix} 0 \\ -ghz_x \\ 0 \end{bmatrix}, \tag{5.29}$$

as

$$\begin{aligned} \bar{U}_{i,j}^{n+\frac{1}{2}} &= U_{i,j}^{n} + \frac{\Delta t}{\Delta x}\left(F^{n}_{i-\frac{1}{2},j} - F^{n}_{i+\frac{1}{2},j} \right) \\ U_{i,j}^{n+\frac{1}{2}} &= \bar{U}_{i,j}^{n+\frac{1}{2}} + \Delta t S(\bar{U}_{i,j}^{n+\frac{1}{2}}) \end{aligned}, \tag{5.30}$$

to get the intermediate solution $U_{i,j}^{n+\frac{1}{2}}$. Using this solution we solve the y-split equations to get the final solution as

$$\begin{aligned} \bar{U}_{i,j}^{n+1} &= U_{i,j}^{n+\frac{1}{2}} + \frac{\Delta t}{\Delta y}\left(G^{n+\frac{1}{2}}_{i,j-\frac{1}{2}} - G^{n+\frac{1}{2}}_{i,j+\frac{1}{2}} \right) \\ U_{i,j}^{n+1} &= \bar{U}_{i,j}^{n+1} + \Delta t S(\bar{U}_{i,j}^{n+1}) \end{aligned}, \tag{5.31}$$

where, G is the numerical flux at the cell interface $j+1/2$ and $j-1/2$ given by

$$G^{n+\frac{1}{2}}_{i,j+\frac{1}{2}} = G\left(U^{n+\frac{1}{2}}_{j+\frac{1}{2}}(0) \right) G^{n+\frac{1}{2}}_{i,j-\frac{1}{2}} = G\left(U^{n+\frac{1}{2}}_{j-\frac{1}{2}}(0) \right). \tag{5.32}$$

5.6 One dimensional test problems

The test problems given by Table 5.1 are introduced by Bernetti *et. al.* (2008). The results are presented in the form of plots for total depth at time $t=1$. The acceleration due to gravity is set to be g = 9.8. In all cases the bottom step is fixed to be 0.2. The bed slope is approximated using the formula (5.25).The results are plotted using 10 cells per unit scale.

Ser.	h_L	h_R	u_L	u_R	z_L	z_R
1	1.461837	0.308732	0.0	0.0	0.0	0.2
2	2.597020	4.62800	0.5	1.5	0.0	0.2
3	0.568999	0.568999	0.9	0.0	0.0	0.2
4	0.50370	0.189824	1.5	0.0	0.0	0.2
5	0.75	1.1	-3.5	-1.5	0.0	0.2
6	0.75	1.1	-0.5	-1.5	0.0	0.2

Table 5.1: One dimensional test cases

Test 1 is a case of combination of shock wave and rarefaction wave. Its solution consists of a rarefaction wave moving towards left, a stationary contact discontinuity and a shock wave moving towards right. The presence of the bottom step forces the reduction of total water height. The solution profile is shown in figure 5.3. Test 2 is the case of divergent flow. The solution contains two rarefaction waves moving apart with stationary contact at the bottom step. The solution profile is shown in the figure 5.4. Test 3 is the case of convergent flow. Its solution consists of two shock waves moving apart with stationary contact at the bottom step. The solution profile is shown in the figure 5.5. Test 4 is the case of supercritical motion from the left. The solution consists of two shock waves moving apart with a middle stationary contact. The solution profile

is shown in the figure 5.6. Test 5 is the case of supercritical motion from right to left. Its solution consists of two rarefaction waves moving opposite to each other. The solution profile is shows in figure 5.7. Test 6 is also the case of supercritical motion from right to left. Its solution results in two shock waves moving apart with a stationary contact at the bottom step. The solution profile is shown in the figure 5.8. The results are compared with the HLLS solver of Murillo et al. (2010). In all the test cases the results obtained are in close agreement with the one obtained in Bernetti *et. al.* (2009).

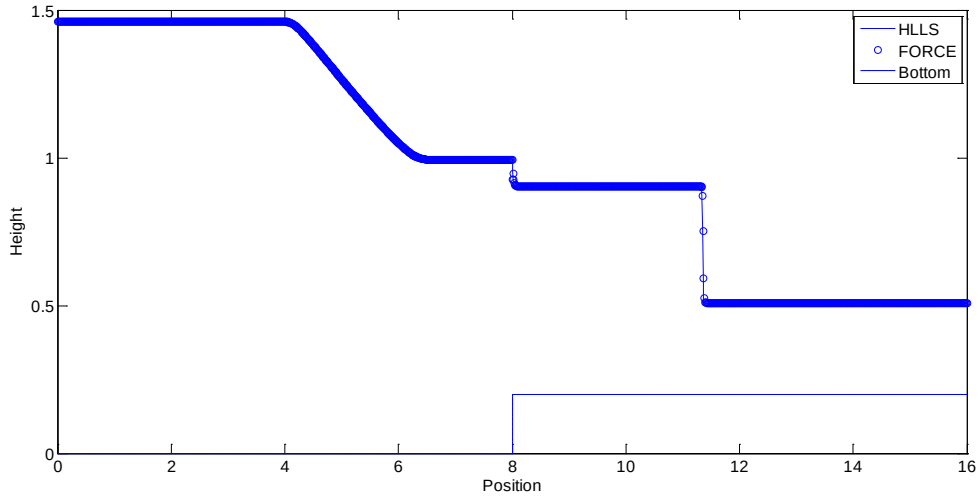

Figure 5.3 Solution profile for test 1

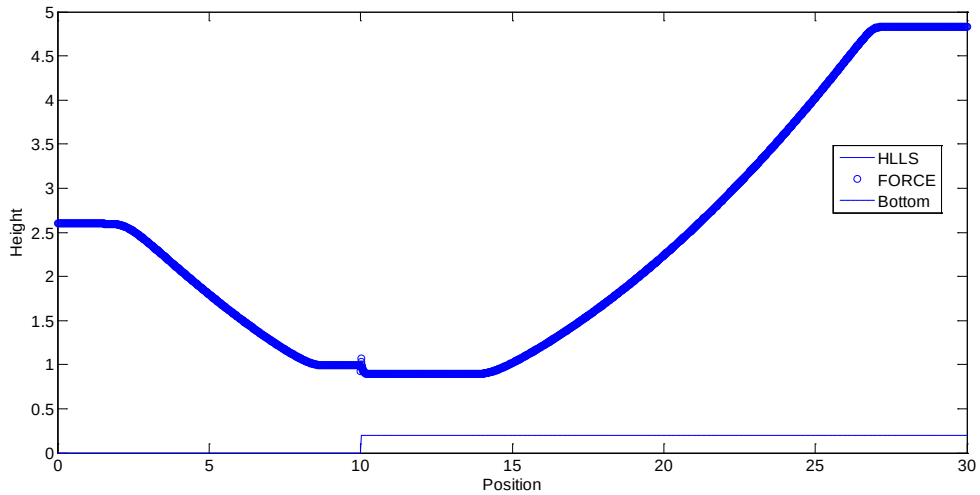

Figure 5.4 Solution profile for test 2

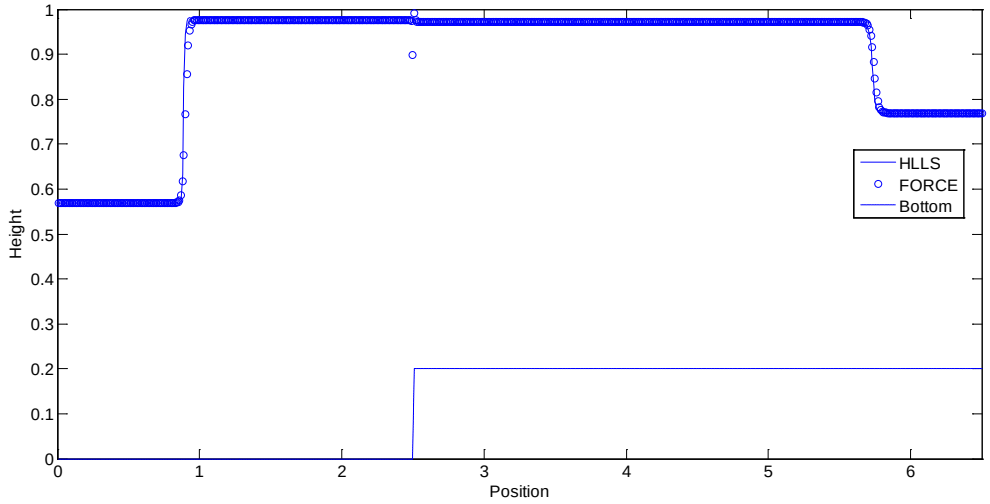

Figure 5.5 Solution profile for test 3

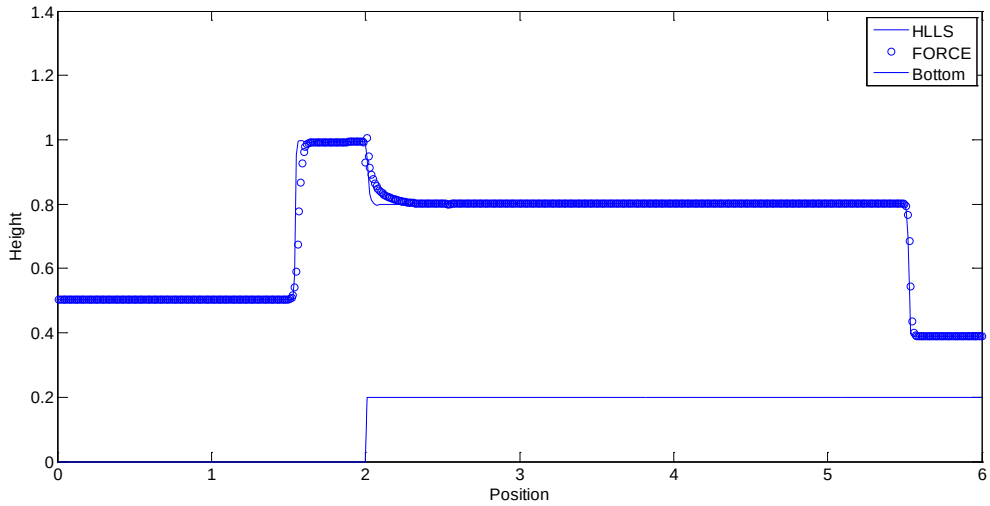

Figure 5.6 Solution profile for test 4

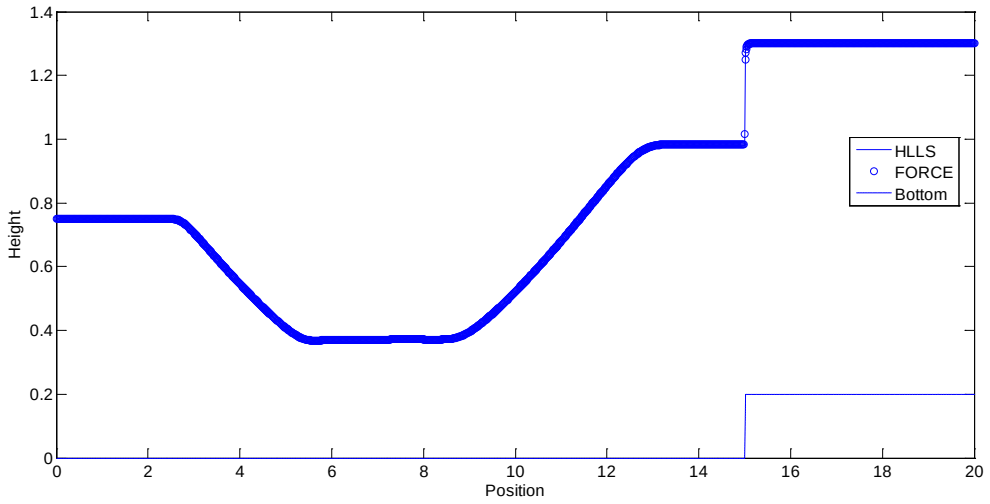

Figure 5.7 Height profile for test 5

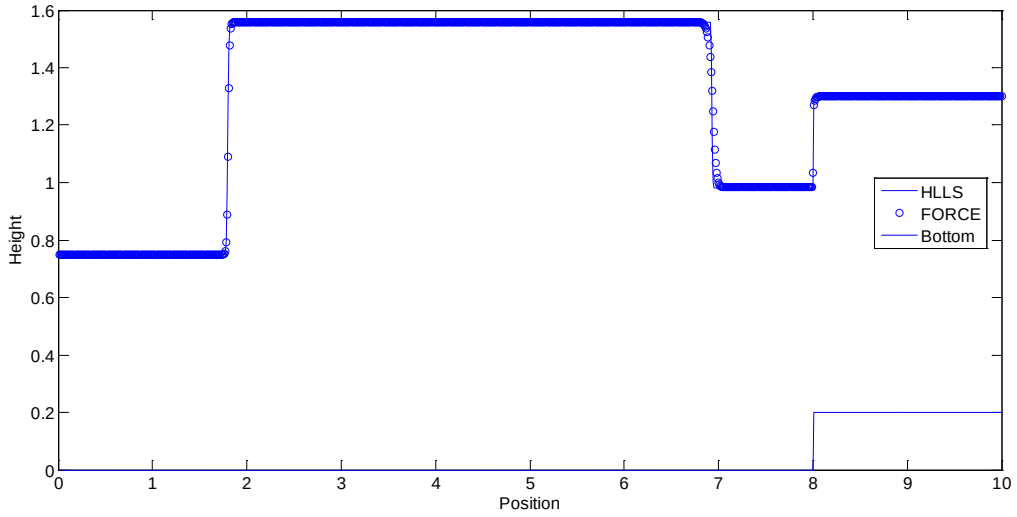

Figure 5.8 Height profile for test 6

5.7 Two dimensional test problems

The computed results for two dimensional cases are presented in the figures 5.9 – 5.18. Test 1 is the circular dam break problem of Himanshu et al., (2015) with variable bottom. Test 2 is the open channel flow with wet bed. Test 3 is the circular dam break problem for dry bed. The data for Test 3 is same as those of test 1 except the region outside the dam is taken to be dry. Test 4 is the modified test 2 for dry bed case. Test 5 is the open channel dam break flow over three humps proposed by Kawahara et al., (1986).

In the circular dam break problem for both the wet bed case and dry bed case, the use of the difference formula (5.25) for bed slope approximation produces an error at the region of stationary discontinuity, see figures 5.9 (a) and 5.11 (a).The use of (5.26) provides more accurate results, see figures 5.9 (b) and 5.11(b). However, In case of purely one dimensional flow, application of (5.26) produces an error in the jump at the stationary discontinuity as can be seen in the figures 5.10 (a) and 5.12 (a). Here the use of (5.25) is suitable, see figures 5.10 (b) and 5.12 (b).

In practical cases with variable bottom geometry, a combination of (5.25) and (5.26), based on the nature of the flow, can be used.

Test 1: Circular Dam Break (wet bed)

The two dimensional circular dam break problem given by Himanshu et al. (2015) is modified to incorporate discontinuous bottom geometry. It consists of a circular dam of radius 10 m located at the centre of a $50\times 50\,m^2$ area filled with water at height $10\,m$. The surrounding area is filled with water at height $3\,m$. Bottom level inside the dam is 0 m and outside it is 1 m. At $t=0s$, the dam is broken and flow is simulated. The initial conditions are given in table 5.2. The obtained results are plotted in figures 5.9(a) and 5.9(b).

X length	$50\,m$
Y length (breadth)	$50\,m$
X Grid Points	500
Y Grid Points	500
CFL Factor	0.90
Centre of Dam (X,Y)	($25\,m$, $25\,m$)
Radius of Circular Dam	$10\,m$
Water Level inside Dam	$10\,m$
Water Level outside Dam	$3\,m$
Bottom Level inside Dam	0
Bottom Level outside Dam	1
X component of initial velocity(Inside)	0
X component of initial velocity(Outside)	0
Y component of initial velocity(Inside)	0
Y component of initial velocity(Outside)	0

Table 5.2: Initial condition for circular dam break (wet bed)

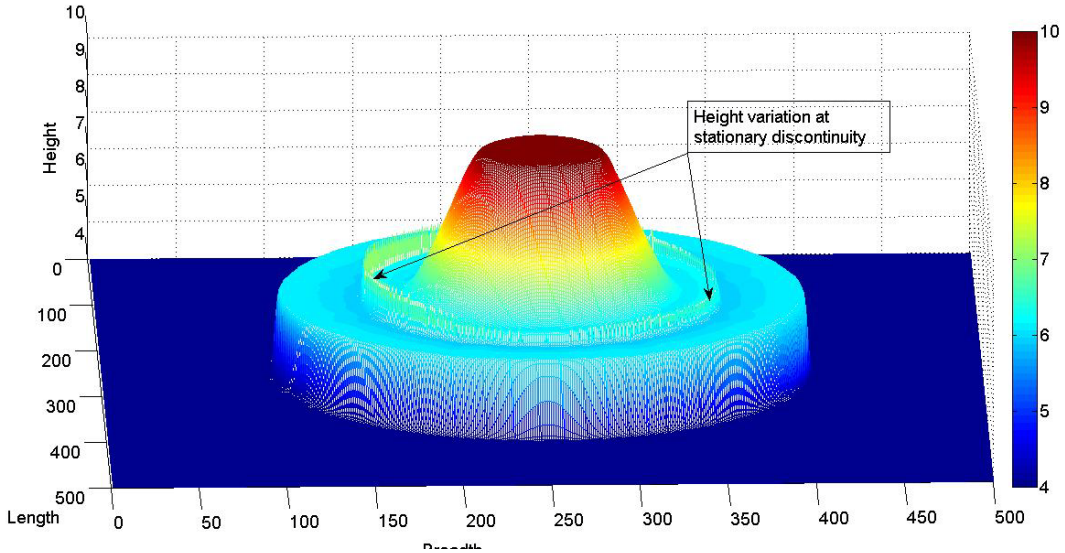

Figure 5.9 (a) Circular dam break at time t = 0.6s with central difference approximation to bottom gradient

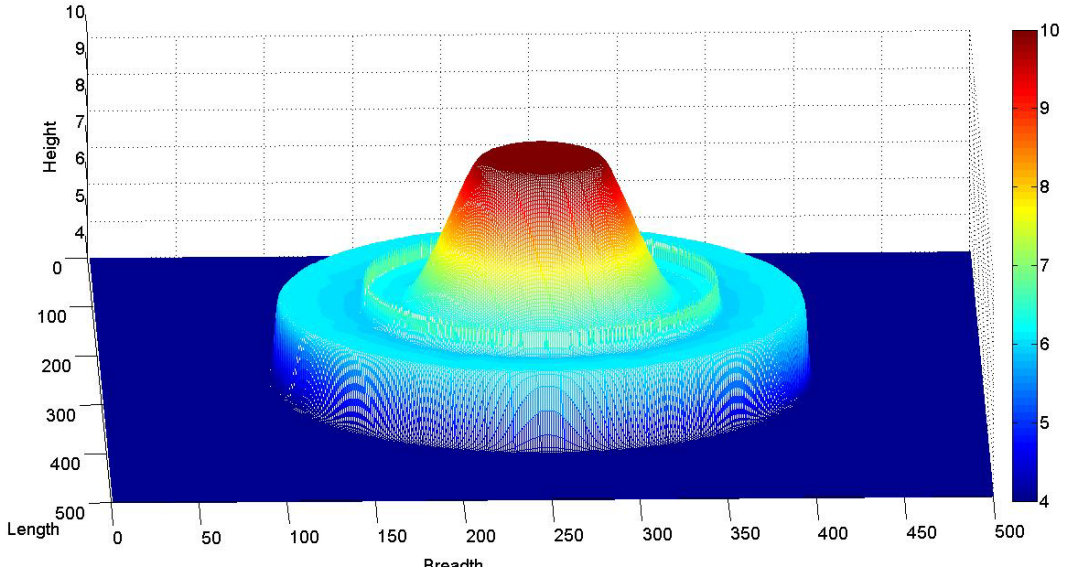

Figure 5.9 (b) Circular dam break at time t = 0.6s with forward difference approximation to bottom gradient

Test 2: The initial conditions and values for the open channel flow (wet bed) are given in Table 5.3 which is a modification of the problem considered in Himanshu et al. (2015) to incorporate bottom geometry.

X length	$50\,m$
Y length (breadth)	$50\,m$
X Grid Points	500
Y Grid Points	500
CFL Factor	0.90
Centre of Dam (X,Y)	$(25\,m\,,\,25\,m\,)$
Location of Dam	$10\,m$
Water Level inside Dam	$10\,m$
Water Level outside Dam	$3\,m$
Bottom Level inside Dam	0
Bottom Level outside Dam	1
X component of initial velocity(Inside)	0
X component of initial velocity(Outside)	0
Y component of initial velocity(Inside)	0
Y component of initial velocity(Outside)	0

Table 5.3: Initial conditions for open channel dam break flow (wet bed)

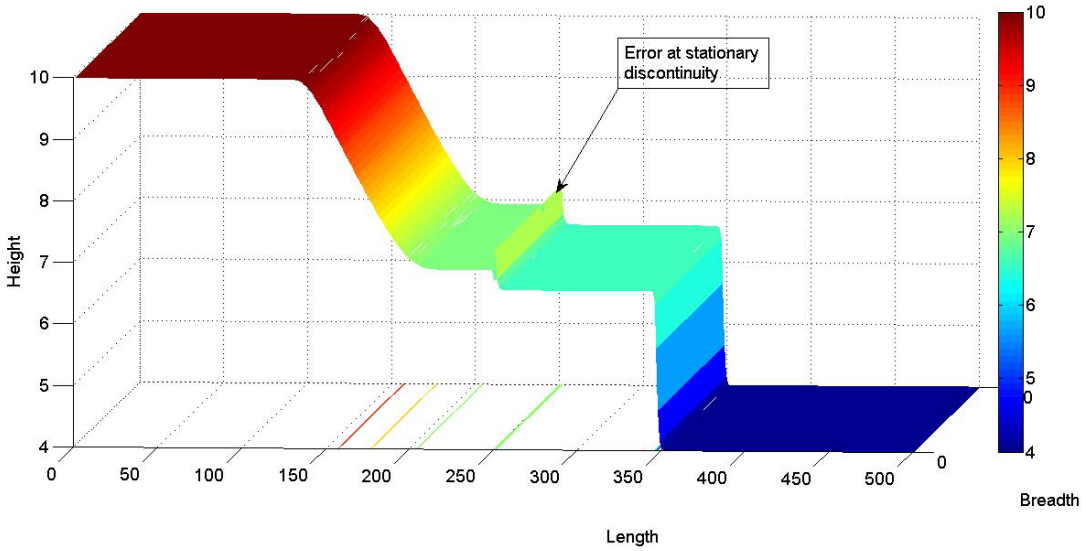

Figure 5.10 (a) Open Channel dam break flow at time t = 1.1s with forward difference approximation to bottom gradient

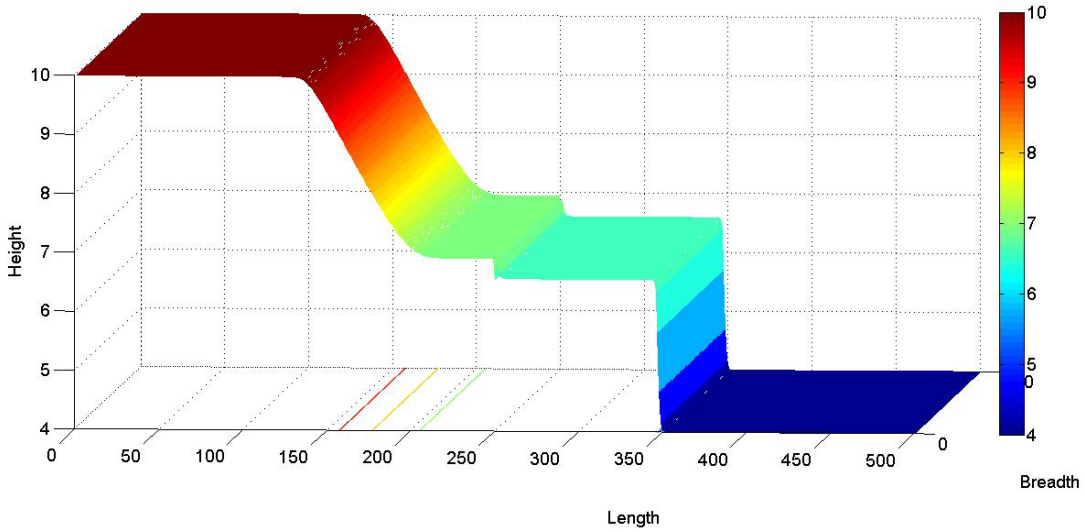

Figure 5.10 (b) Open Channel dam break flow at time t = 1.1s with central difference approximation to bottom gradient

Test 3: The initial conditions and values for the Circular Dam Break (dry bed) are given in Table 5.4. It is a modification of test 1 for dry bed case.

X length	$50\,m$
Y length (breadth)	$50\,m$
X Grid Points	500
Y Grid Points	500
CFL Factor	0.90
Centre of Dam (X,Y)	$(25\,m\,,\,25\,m\,)$
Radius of Circular Dam	$10\,m$
Water Level inside Dam	$10\,m$
Water Level outside Dam	$0\,m$
Bottom inside Dam	$0\,m$
Bottom outside Dam	$1\,m$
X component of initial velocity(Inside)	0
X component of initial velocity(Outside)	0
Y component of initial velocity(Inside)	0
Y component of initial velocity(Outside)	0

Table 5.4: Initial condition for circular dam break (dry bed)

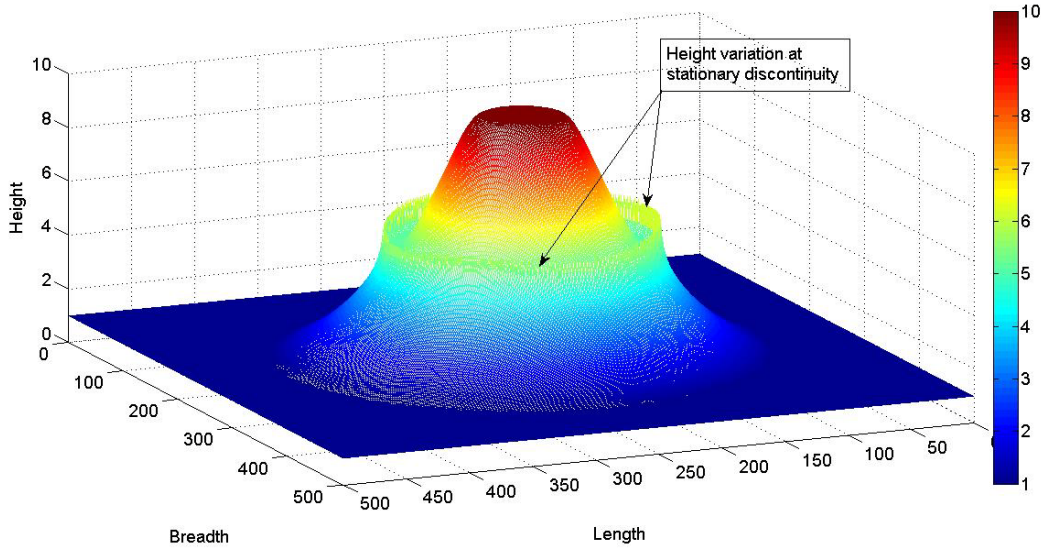

Figure 5.11 (a) Circular dam break at t = 0.6s with central difference approximation to bottom gradient

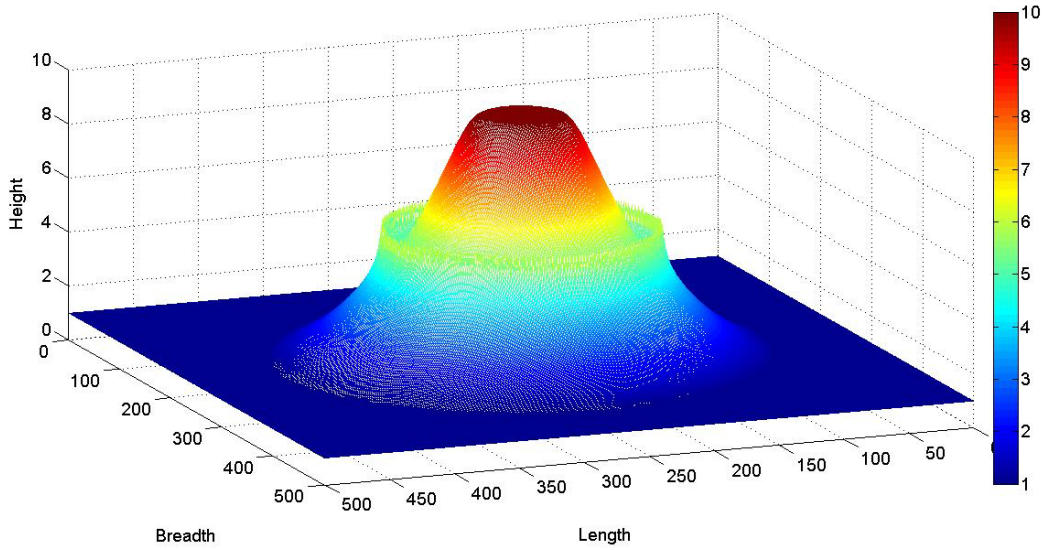

Figure 5.11 (b) Circular dam break at t = 0.6s with forward difference approximation to bottom gradient

Test 4: The initial conditions and values for the open channel dam break flow (dry bed) are given in Table 5.5. It is a modification of test 2 for dry bed case.

X length	$50\,m$
Y length (breadth)	$50\,m$
X Grid Points	500
Y Grid Points	500
CFL Factor	0.90
Centre of Dam (X,Y)	$(25\,m\,,\,25\,m\,)$
Location of Dam	$10\,m$
Water Level inside Dam	$10\,m$
Water Level outside Dam	$0\,m$
Bottom inside Dam	$0\,m$
Bottom outside Dam	$1\,m$
X component of initial velocity(Inside)	0
X component of initial velocity(Outside)	0
Y component of initial velocity(Inside)	0
Y component of initial velocity(Outside)	0

Table 5.5: Initial conditions for open channel dam break flow (dry bed)

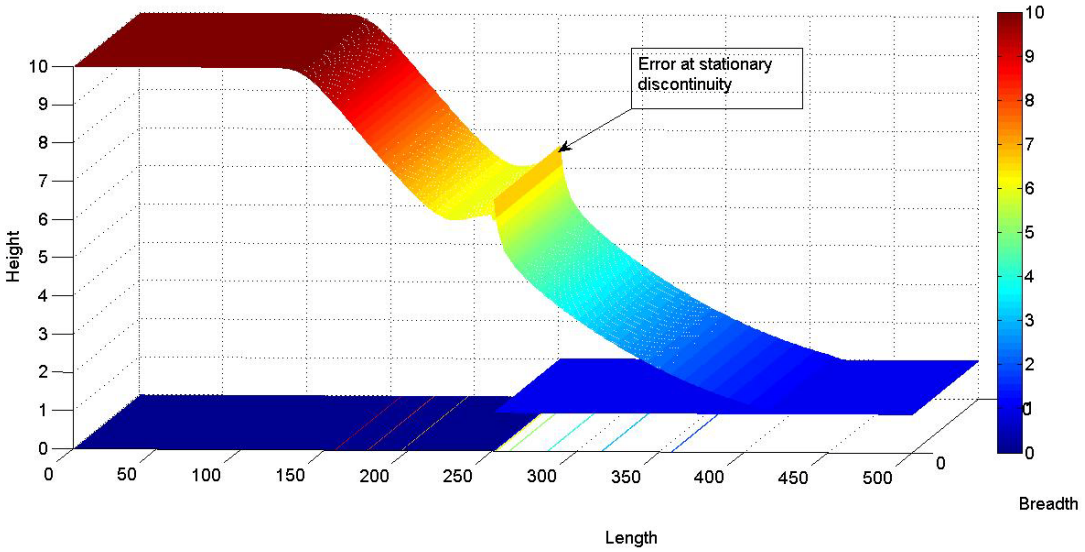

Figure 5.12 (a) Open channel dam break flow at t = 1.1s with forward difference approximation to bottom gradient

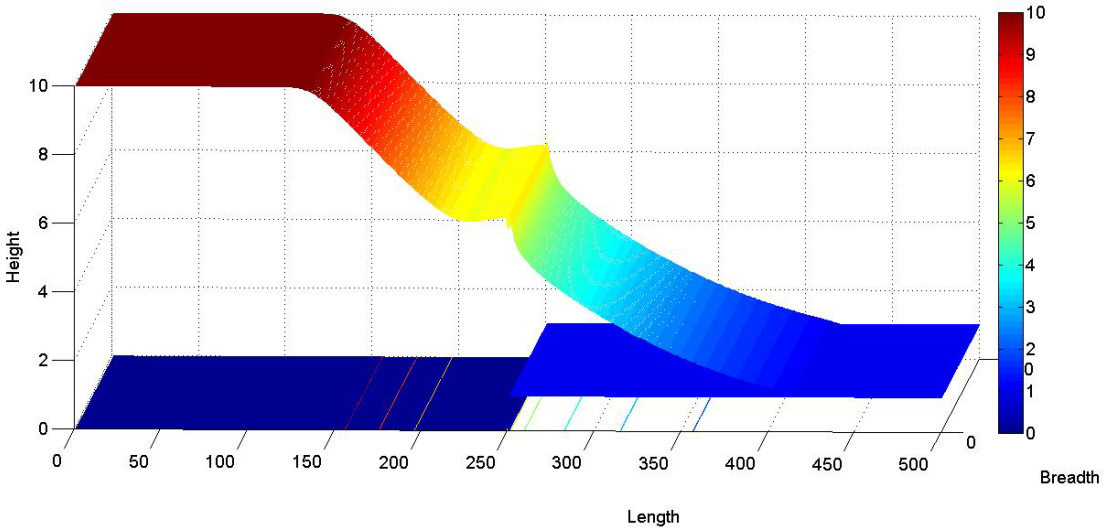

Figure 5.12 (b) Open channel dam break flow at t = 1.1s with forward difference approximation to bottom gradient

Test 5: Dam break waves propagating over three humps:

Consider the case of a dam break wave travelling over an initially dry flood plain with three humps, proposed by Kawahara and Umetsu (1986), and has been reexamined by other authors such as Liang et al. (2009) and Brufau et al., (2002). The initial conditions and values for this problem are given in Table 5.6.

X length	$75\,m$
Y length (breadth)	$30\,m$
X Grid Points	750
Y Grid Points	300
CFL Factor	0.90
Centre of Dam (X,Y)	$(37.5\,m\,,\,15\,m\,)$
Location of Dam	$16\,m$
Water Level inside Dam	$1.875\,m$
Water Level outside Dam	$0\,m$
Bottom inside Dam	$0\,m$
Bottom outside Dam	3 humps given below
X component of initial velocity(Inside)	0
X component of initial velocity(Outside)	0

Table 5.6: Initial conditions for open channel flow with three humps

Here the dam break is considered to occur in a 75 m long and 30 m wide container, which has the bottom geometry given by

$$z(x,y)=\max\left[0,1-\frac{1}{8}\sqrt{(x-30)^2+(y-6)^2},1-\frac{1}{8}\sqrt{(x-30)^2+(y-24)^2},3-\frac{3}{10}\sqrt{(x-47.5)^2+(y-15)^2}\right].$$

Initially, the still water of height $h=1.875m$ is retained in the container with the dam located at $x=16\ m$. The results obtained are same as those obtained by Brufau at al., (2002) and Yulong (2005), and are discussed below.

Figure 5.13 illustrates the bottom geometry within the computational domain and the upstream still water supported by the dam. The bed slope is approximated by using central difference formula (5.26). At $t=0$, dam collapses catastrophically. Figures 5.14 – 5.18 illustrates the inundated floodplain at various time levels including the time at which steady state is reached. Three dimensional plots of the water surface, plain view of water depth plots are given. A moment after the dam break, a flood wave with a wet-dry front starts to inundate the floodplain. At the time $t=2s$, the wet dry front has reached the small mounds and rose above them and a curved shock is created at the small mounds. At the same time part of the wet-dry front continues to advance between the mounds. When the time reaches $t=6s$ the small mounds are entirely inundated, and due to momentum of the flood wave, the wet-dry front has started to rise over top of the large mound and starts descending. The curved shocks continue to move upstream and started to interact with each other and the side walls of the container. When time reaches $t=12s$, the flood water that was passing through the sides of the large mound starts to converge behind the large mound. The upstream directed curved shock-waves from the small mounds have consolidated into a nearly straight bore. The water level at the large mound reduced as the reflection bore moves farther. After sophisticated wave-wave, wave-wall and wave topography interactions, the flow starts to culminate into steady

state. The steady state is reached at $t = 300s$. At this time the peaks of the small mounds are no longer submerged. The numerical model properly simulates complicated wetting and drying processes and produces the results that are very similar to those of Brufau *et. al.* (2002) and Liang *et. al.* (2009).

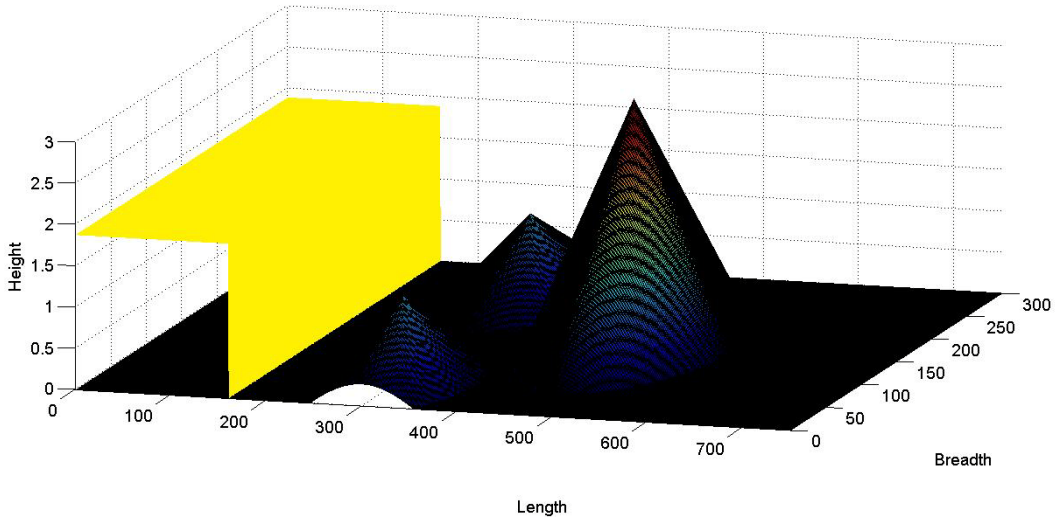

Figure 5.13 Initial State, at time t = 0s

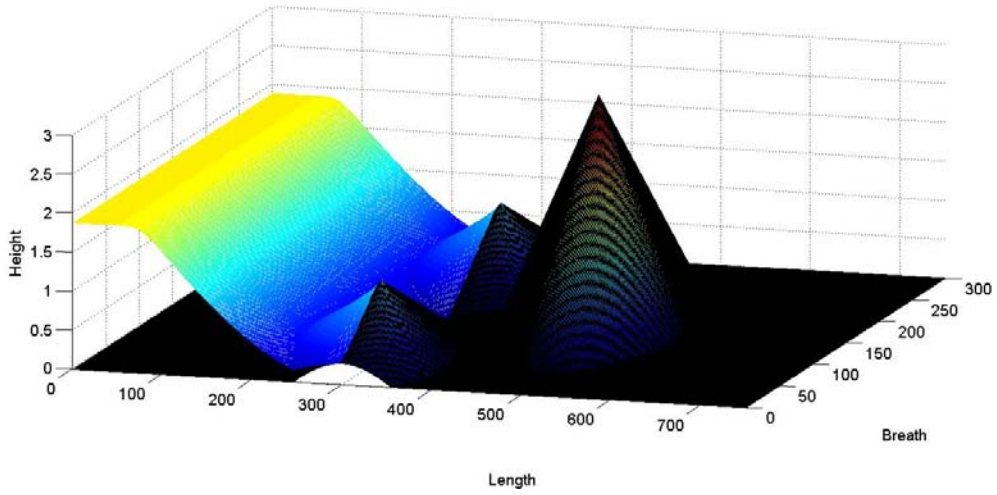

Figure 5.14(a) Profile at time t = 2s

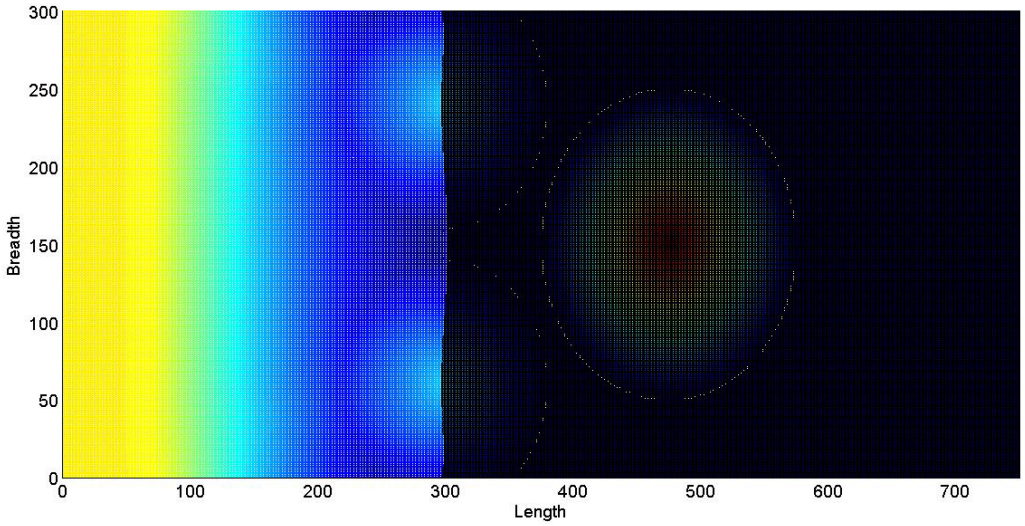

Figure 5.14(b) Plane view of profile at time t = 2s

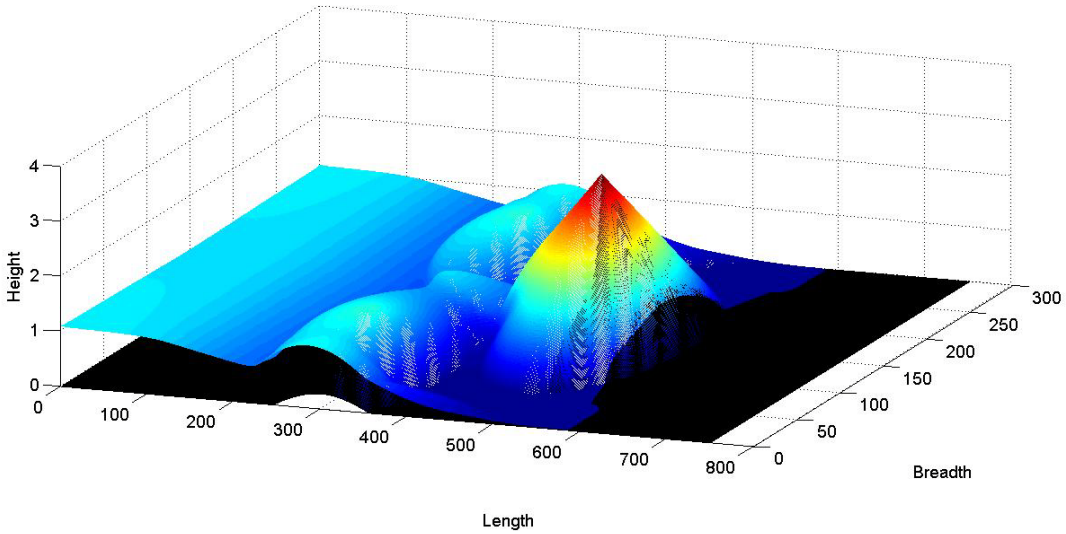

Figure 5.15(a) Profile at time t = 6s

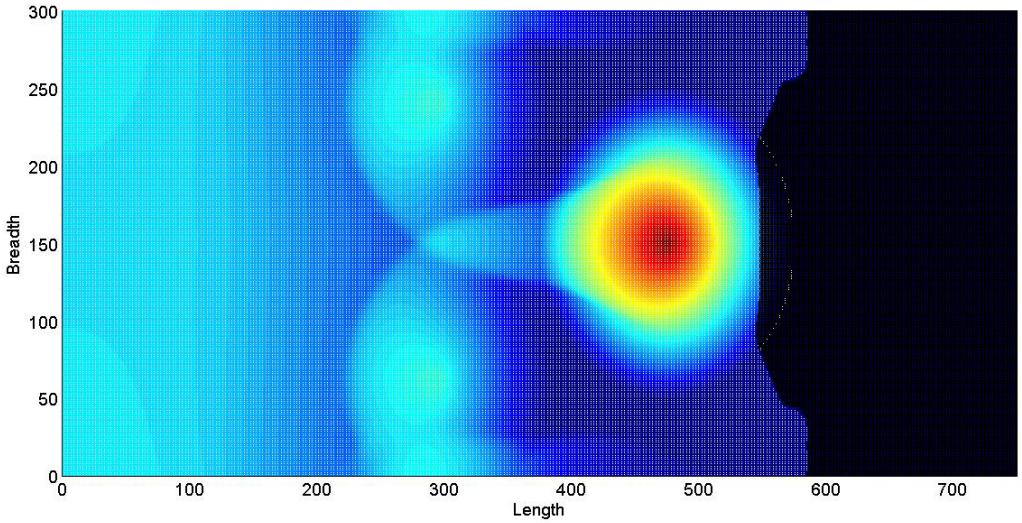

Figure 5.15(b) Plane view of profile at time t = 6s

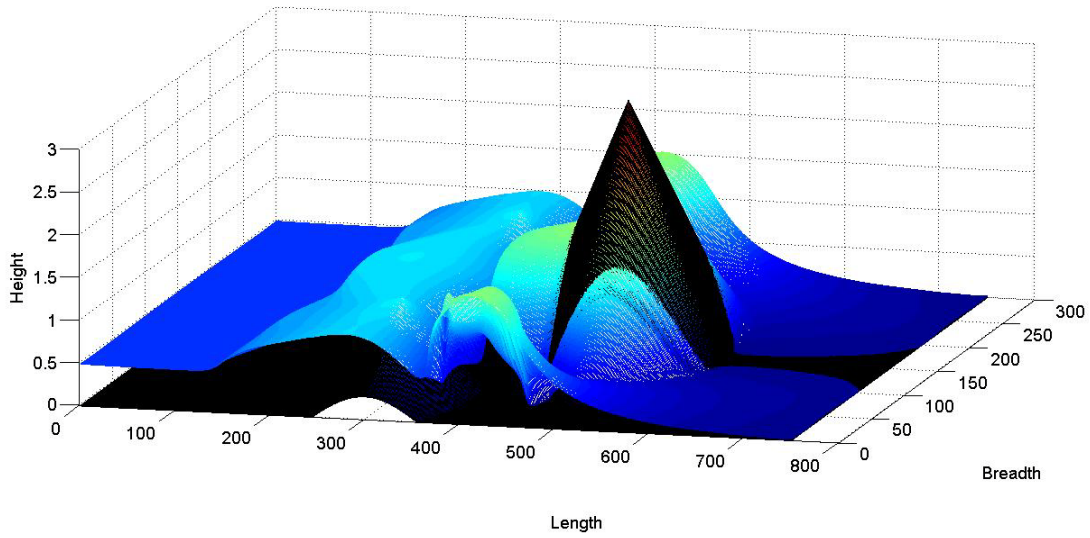

Figure 5.16(a) Profile at time t = 12s

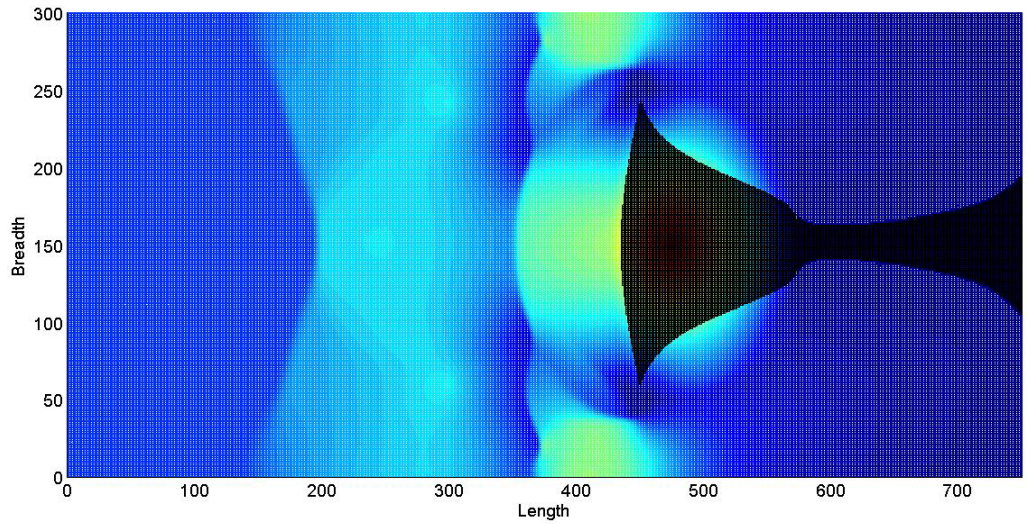

Figure 5.16(b) Plane view of profile at time t = 12s

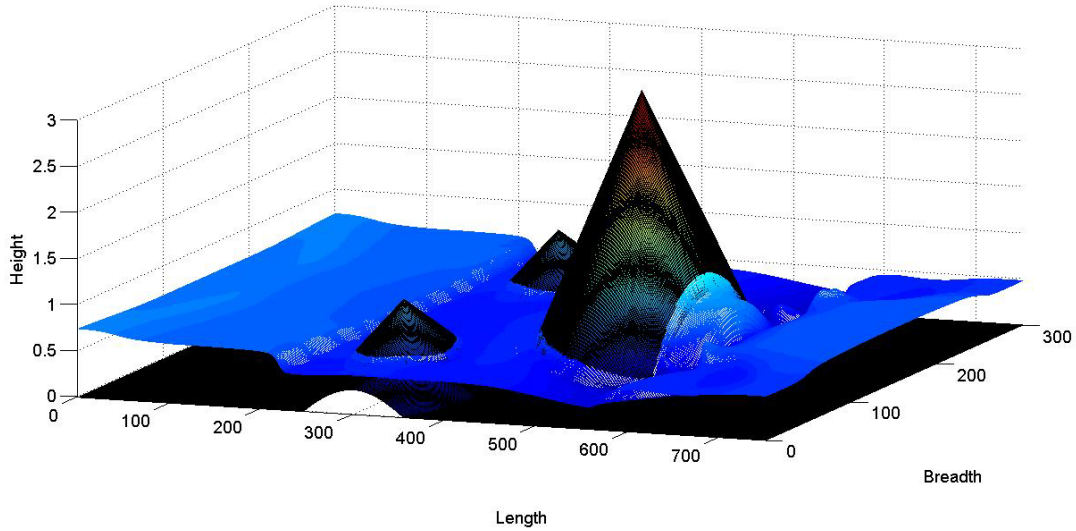

Figure 5.17(a) Profile at time t = 30s

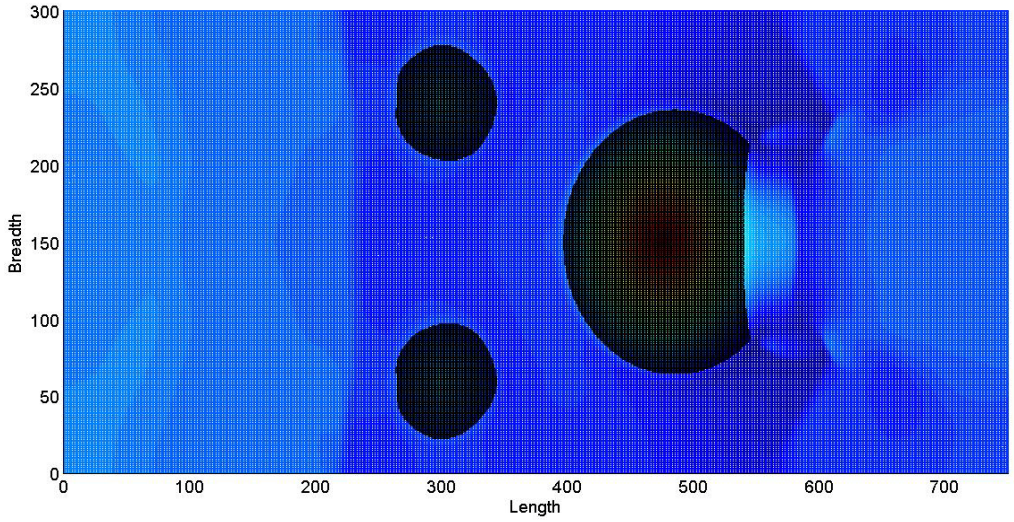

Figure 5.17(b) Plane view of profile at time t = 30s

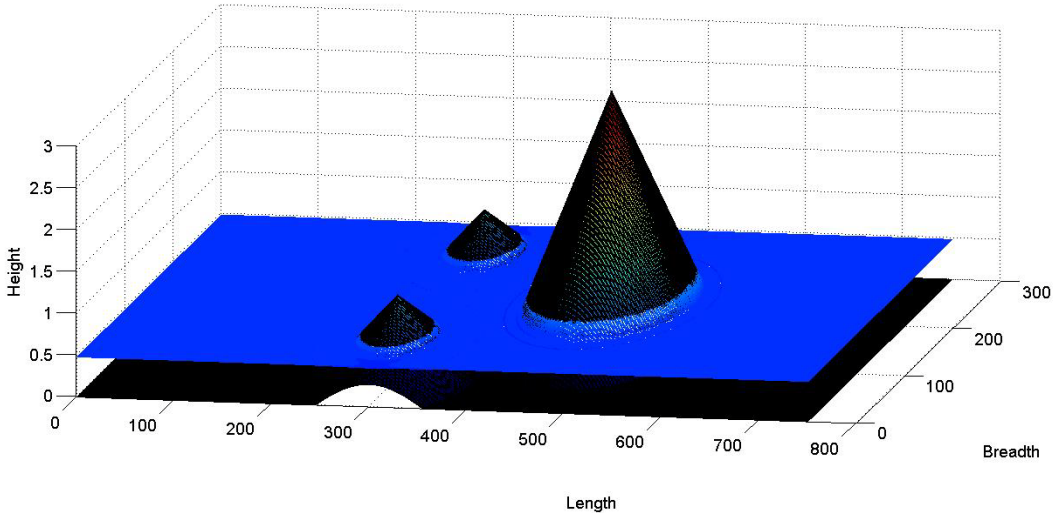

Figure 5.18(a) Profile at time t = 300s

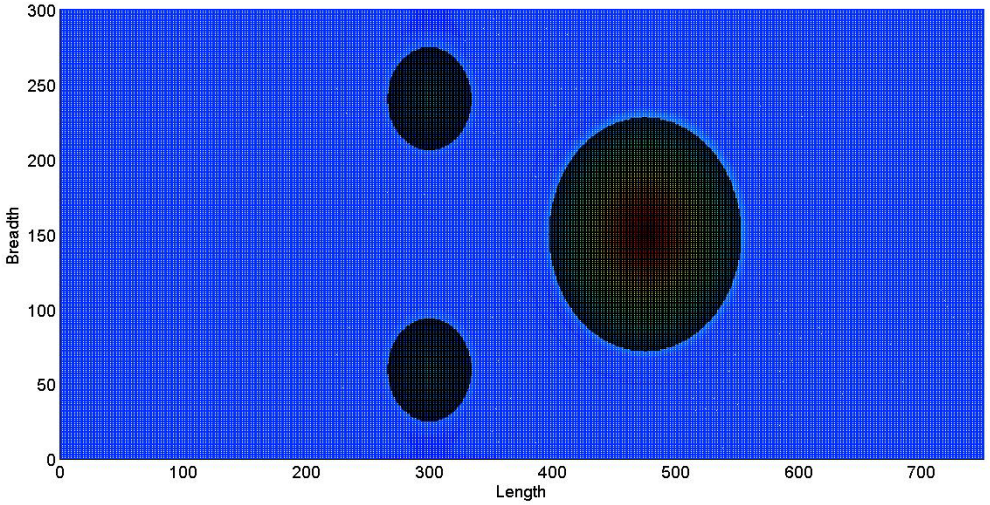

Figure 5.18(b) Plane view of profile at time t = 300s

5.8 Conclusions

The present chapter deals with the numerical solution of two dimensional shallow water equations with variable bottom geometry. FORCE method is used to numerically simulate the shallow water equation using operator splitting procedure. Although the FORCE scheme is first order, the test problems show that the method is applicable to the flow with variable bottom. FORCE method with operator splitting is able to treat the wet/dry front and complex wave interactions. The solutions obtained by numerical simulation are in agreement with the analytical solutions and numerical predictions. It is also shown that the treatment of source term depends on the geometry of the problem. It is intended that FORCE method with operator splitting can be applied to practical problems with complex geometries.